Lab on a Chip

Cite this: *Lab Chip*, 2012, **12**, 4003–4005

www.rsc.org/loc

HIGHLIGHT

Research Highlights

Šeila Selimović,[ab] MD Anwarul Hasan,[ab] Mehmet R. Dokmeci[ab] and Ali Khademhosseini*[abcd]

DOI: 10.1039/c2lc90101c

Blood vessels on-chip

The ability to generate blood vessels can be used to generate tissues for therapeutics[1] as well as a range of other applications.[2] One such application is the development of blood vessels on-chips for drug discovery applications.

Recently, progress has been made by Jeon and colleagues in developing blood vessels on a chip within a microfluidic device,[3] along with an increasing number of other works in the same area.[4] In particular, by utilizing a mixture of fibrin and collagen-based gels and optimizing the environmental conditions, Yeon *et al.*[3] demonstrated the formation of complete vascular channels.

The poly(dimethylsiloxane) (PDMS) device in this example consisted of two main parallel channels, connected with an array of narrow bridging channels of varying dimensions (~100 μm wide and up to 1.6 mm long, Fig. 1a–c). Yeon *et al.*[3] then introduced a gel precursor mixture of fibrin and collagen into these bridging channels and crosslinked it. The main channels were then perfused with cell media, which also penetrated into the gels, and were filled with human umbilical vein endothelial cells (HUVECs) and fibroblasts. While HUVECs attached to the edges of the gel, fibroblasts lined the walls of the main channels.

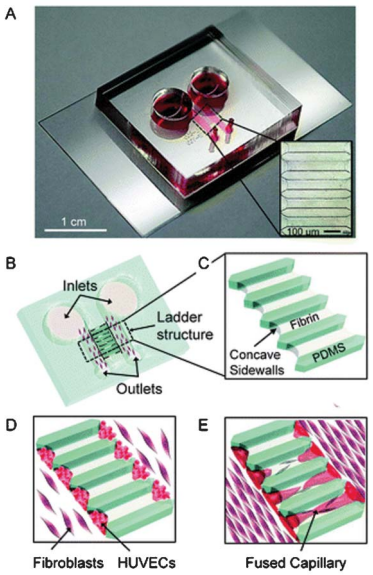

Fig. 1 Microfluidic device and capillary formation: (A) image of the assembled device with the expanded view of the gel-filled bridging channels; (B) device schematic; (C) enlarged sketch of the bridging channels (white) filled with a fibrin-collagen mixture; (D) sketch of the channel structure with HUVECs (red) and fibroblasts (purple); (E) spontaneously formed vascular HUVEC networks. Figure reprinted with permission from the Royal Society of Chemistry from Yeon *et al.*[3]

Within a short time, HUVECs attached to the gels and began to migrate into the gel-filled bridging channels (Fig. 1d). After a few days of culture, cells sprouting into the gels from both sides fused with each other and formed vascular structures (Fig. 1e). This was indicated by the tight junction protein (*e.g.* ZO-1) barrier function. In addition, lumen-like structures could be observed.

The shape of the bridging channels had a strong effect on the formation of the vascular network. Specifically, adequate vascular sprouting was only observed in channels that were wider at the inlet than at the center, as this facilitated the adhesion of a large number of HUVECs. Interestingly, the presence of fibroblasts in close proximity to HUVECs was also found to be essential for lumen formation. This is most likely due to the secretion of paracrine factors by these cells that are important for angiogenesis. The ability to generate a vascular network was also dependent on the ratio of fibrin to collagen. At high ratios of fibrin to collagen, HUVECs could not penetrate deep into the gel, whereas at low ratios the gels detached from the PDMS and were washed away during perfusion. Thus an optimum concentration was required to obtain vessel-like structures.

A drawback of the experimental system is its sensitivity to a range of parameters. The number of attached HUVECs, the distance between HUVECs and fibroblasts, as well as the shape and size of the gel-filled bridging structures, had to be within an optimal range to allow for vascular network formation. Furthermore, the authors had limited control over the size and shape of the formed lumen.

Nonetheless, the results of the study offer useful insights into spontaneous vascularization that will be helpful in other blood vessel on a chip applications, especially since these blood vessels are accessible and perfusable. This microfluidic device could potentially enable the study of angiogenesis related to wound healing, aging, cancer metastasis and pathogenesis. In the future, replacing the PDMS structure with a suitable

[a]*Center for Biomedical Engineering, Department of Medicine, Brigham and Women's Hospital, Harvard Medical School, Cambridge, Massachusetts 02139, USA. E-mail: alik@rics.bwh.harvard.edu*
[b]*Harvard-MIT Division of Health Sciences and Technology, Massachusetts Institute of Technology, Cambridge, Massachusetts 02139, USA*
[c]*Wyss Institute for Biologically Inspired Engineering, Harvard University, Boston, Massachusetts 02115, USA*
[d]*World Premier International-Advanced Institute for Materials Research (WPI-AIMR), Tohoku University, Sendai 980-8577, Japan*

biodegradable alternative could potentially render the final vascularized construct implantable into living tissue for *in vivo* experiments.

Smart implants for diabetes treatment

Type 1 diabetes is a chronic condition in which the pancreas does not produce enough insulin, a hormone that regulates the levels of glucose in blood by storing it in muscle, fat and liver cells. Insulin replacement therapy is the standard treatment for this disease.[5] Insulin is commonly administered through injections, and blood sugar levels are tested several times per day using point-of-care sensors that collect blood from a finger-prick. Less accurate, though more convenient, are implantable glucose sensors that rely on the interstitial fluid instead of blood as samples. The results are transmitted to (external) insulin pumps.[6]

Efforts to develop a highly accurate, continuously operating and fully implantable sensing and treatment device that will improve the patients' quality of life have recently been undertaken by Giacca, Wu, Sun and coworkers. Chu *et al.*[7] utilized a previously developed[8] bioinorganic membrane containing pH-responsive nanoparticles to simultaneously detect glucose and allow insulin to permeate out of a storage reservoir. The improvement efforts in the present work focused on incorporating this membrane into a structurally robust device that coupled a large membrane surface for increased insulin permeation with an enlarged insulin reservoir. These modifications enabled the generation of a stand-alone, implantable device that contained enough insulin to control the glucose levels over several days in diabetic rats.

The bioinorganic membrane was attached to a small (1 cm diameter) PDMS container covered with a PDMS-grid layer for structural support (Fig. 2a). Poly(ethylene glycol) coating was applied to the hydrophobic PDMS to increase its biocompatibility for *in vivo* studies. The membrane was based on alginate and contained embedded MnO_2 and PNIPAM–PMAA (poly(*N*-isopropyl-acrylamide)–poly(methacrylic acid)) nanoparticles. The magnesium-based nanoparticles were incorporated to aid in replenishing the oxygen consumed during glucose oxidation, while the hydrogel nanoparticles responded to the changes in pH due to production of gluconic acid (also a result of glucose oxidation). Increasing glucose levels leads to a reduction in environmental pH, causing the nanoparticles to collapse (Fig. 2b). As a consequence, the membrane pore size increases, allowing insulin to permeate out of the reservoir through the membrane into the surrounding space and interact with glucose. Alternatively, a reduction in blood sugar levels causes a spike in pH and the nanoparticles swell, obstructing the insulin permeation path. Thus, the nanoparticles were described by the authors as "intelligent valves".

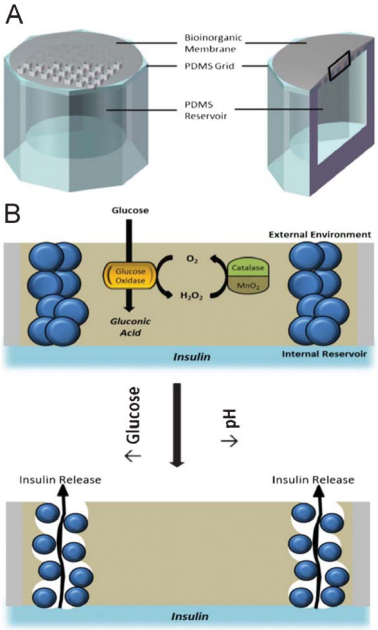

Fig. 2 Schematic of the glucose-sensing insulin delivery device (A). Nanoparticles embedded into the membrane respond to increased glucose concentrations by shrinking, enabling the release of insulin from the reservoir into the environment (B). Figure adapted and reprinted with the permission from the Royal Society of Chemistry from Chu *et al.*[7]

The performance of this "smart" device was investigated both *in vitro* and *in vivo*. In both cases the device quickly responded to a four-fold increase in glucose levels by discharging insulin, reducing the concentration of blood sugar to the normoglycemic range within half an hour, and then stopped delivering the hormone. The accuracy of this response was maintained over several cycles in glucose spikes. Moreover, the device was reliably operational for up to ten days, *ex vivo* and after implantation into diabetic rats. Measurements of a particular plasma protein indicated that the changes in insulin levels detected in rat blood were caused by the microdevice and not by a normal physiological response.

This smart insulin-delivery device represents an important advance in the development of implantable, closed-loop platforms for the study and treatment of diabetes. The current proof-of-concept version of the device will likely permit short-term studies of glucose metabolism disorders in animals. Since diabetes is a chronic disease, however, it would be beneficial to modify the present approach to enable longer-term regulation of glucose levels, in order to reduce the frequency of invasive implantation procedures.

Particles in microchannels as active flow elements

Microscale flows in the laminar flow regime are often treated as insensitive to the presence of suspended particles. This is the regime of low Reynolds number Re ($\ll$2300), the ratio of inertial to viscous forces. Indeed, it is often assumed that the suspended particles translated by the main flow are passive, such that any fluid packets shifted by the flowing particles return to their initial streamlines (Stokes' flow).[9] This premise ignores the inertial effects of the fluid around the particles. In reality, however, particles with relatively large particle Reynolds numbers (Re_p>1, describing the effect on the surrounding flow) do influence the fluid packets around them. Namely, the particles can occupy large volumes inside fluidic channels, creating significant fluid disturbances. In addition, inertial effects of the fluid due to the velocity gradients across the particles become more important with decreasing channel dimensions.[10] While particle–particle interactions in fluids have long been a topic of research, particle–fluid interactions due to fluid inertia differences across a particle in small fluidic channels are only recently coming into focus.[11]

Di Carlo and colleagues have recently completed a study of secondary flows inside microfluidic channels that arise as

a consequence of the suspended particles. Amini *et al.*[12] compared the pressure-driven flow surrounding a hydrodynamically focused, rotating (due to its off-center position), translating particle, with and without the effects of particle inertia. This was accomplished through a finite element method simulation based on incompressible Navier–Stokes equations in a 3D microfluidic channel, in the particle's frame of reference.

In both cases – confined Stokes' and inertial flows – reversing streamlines were observed near the channel walls. However, a net secondary or convection flow was only detected in the inertial case. While in Stokes' flow the transverse fluid transport upstream and downstream of the particle was symmetric, resulting in no net fluid transfer, in the inertial flow it lagged the Stokes' situation. The difference in these convection flows was greater upstream than downstream, causing a net fluid transfer. The intensity of the secondary flow was shown to scale as the cube of the particle diameter and the square of the flow velocity, and it was linearly related to the fluid density. Furthermore, a reduction in channel width (and the corresponding increase in velocity gradient) and increase in height (larger mass transport) both led to greater convection flow velocities.

The numerical work was supplemented with experiments demonstrating the particle-induced secondary flows. To this end, a simple microfluidic channel was constructed with two inlet ports, for the co-flow of a dye solution and a clear, dilute particle suspension. Polystyrene particles with diameters that ranged from 1/2 to 2/3 of the channel width (w = 70 μm) were flowed in the clear stream through the system and the changes in streamlines were captured using a high-speed camera. The predicted flow disturbance was indeed observed, as was the particle rotation. Quantitative measurements of the convective flow were gathered in a similar setup from a 60 μm wide channel that was filled with monodisperse 10 μm PDMS spheres in a clear solution and a co-flowing fluorescent stream. At high flow rates (300 μl min^{-1}) and high Re_p (>2) the convection was sufficiently strong to distribute both streams along the full channel width. This result was captured in a high transport factor (TF) of the dyed solution (TF = 1). At Re_p>1 and without the presence of particles, however, the mixing of the dyed and clear solutions was driven by diffusion alone, resulting in a much lower TF (0.5).

This convectively driven exchange of fluids was exploited for cell washing (cancer cells and leukocytes) and mixing of blood with a buffer solution. In both cases a relatively high cell fraction (~25%) was required to induce the convective exchange of liquids, while avoiding crowding effects.

The inertial secondary flows were discovered to arise from the relative translation and rotation of the particle compared to the underlying flow and confinement due to neighboring channel walls. Importantly, these flows do not feed back to the particles, and the particles remain focused on their equilibrium streamlines. Thus, this convective mechanism could be utilized for mixing at high flow velocities and other mass transport applications such as fluid exchange around beads, cell lysis and particle washing.

References

1 R. Sudo, S. Chung, I. K. Zervantonakis, V. Vickerman, Y. Toshimitsu, L. G. Griffith and R. D. Kamm, *FASEB J.*, 2009, **23**, 2155–2164.
2 E. C. Novosel, C. Kleinhans and P. J. Kluger, *Adv. Drug Delivery Rev.*, 2011, **63**, 300–311.
3 J. H. Yeon, H. R. Ryu, M. Chung, Q. P. Hu and N. L. Jeon, *Lab Chip*, 2012, **12**, 2815–2822.
4 J. W. Song and L. L. Munn, *Proc. Natl. Acad. Sci. U. S. A.*, 2011, **108**, 15342–15347.
5 D. E. DeWitt and I. B. Hirsch, *JAMA, J. Am. Med. Assoc.*, 2003, **289**, 2254–2264.
6 T. J. D. R. F. C. G. M. S. Group, *N. Engl. J. Med.*, 2008, **359**, 1464–1476.
7 M. K. L. Chu, J. Chen, C. R. Gordijo, S. Chiang, A. Ivovic, K. Koulajian, A. Giacca, X. Y. Wu and Y. Sun, *Lab Chip*, 2012, **12**, 2533–2539.
8 C. R. Gordijo, A. J. Shuhendler and X. Y. Wu, *Adv. Funct. Mater.*, 2010, **20**, 1404–1412.
9 L. E. Payne and W. H. Pell, *J. Fluid Mech.*, 1960, **7**, 529–549.
10 B. Kirby, *Micro- and Nanoscale Fluid Mechanics*, Cambridge University Press, Cambridge, 2010.
11 A. S. Sangani, A. Acrivos and P. Peyla, *Phys. Fluids*, 2011, **23**, 083302.
12 H. Amini, E. Sollier, W. M. Weaver and D. D. Carlo, *Proc. Natl. Acad. Sci. U. S. A.*, 2012, **109**, 11593–11598.